IITM High-Resolution Global Forecast Model Version 1: An attempt to resolve monsoon prediction deadlock

R. Phani Murali Krishna[1], Siddharth Kumar[1], A. Gopinathan Prajeesh[2], Peter Bechtold[3], Nils Wedi[3], Kumar Roy[4], Malay Ganai[1], B. Revanth Reddy[1], Snehlata Tirkey[1], Tanmoy Goswami[1], Radhika Kanase[1], Sahadat Sarkar [1], Medha Deshpande[1], Parthasarathi Mukhopadhyay [1,5]

[1]Indian Institute of Tropical Meteorology, Ministry of Earth Sciences, Dr. Homi Bhabha Road, Pune 411008, India
[2] King Abdullah University of Science and Technology, Saudi Arabia
[3] ECMWF
[4] University of Victoria, Canada
5 Department of Earth and Environmental Sciences, Indian Institute of Science Education and Research, Berhampur 760003, Odisha, India

Correspondence to: Dr. P. Mukhopadhyay (mpartha@tropmet.res.in; parthasarathi64@gmail.com)

Abstract. The prediction of Indian monsoon rainfall variability, affecting a country with a population of billions, remained one of the major challenges of the numerical weather prediction community. While in recent years, there has been a significant improvement in predicting the synoptic scale transients associated with the monsoon circulation, the intricacies of rainfall variability remained a challenge. Here, an attempt is made to develop a global model using a dynamic core of a cubic octahedral grid that provides a higher resolution of 6.5 km over the global tropics. This high-resolution model has been developed to resolve the monsoon convection. Reforecasts with the IITM High-resolution Global Forecast Model (HGFM) have been run daily from June through September 2022. The HGFM model has a wavenumber truncation of 1534 in the cubic octahedral grid. The monsoon events have been predicted with a ten-day lead time. The HGFM model is compared to the operational GFS T1534. While the HGFM provides skills comparable to the GFS, it shows better skills for higher precipitation thresholds. This model is currently being run in experimental mode and will be made operational.

1 Introduction

In spite of significant improvement in numerical weather prediction skills in the last decades (Bechtold et al., 2008; Magnusson and Kallen, 2013; Hoffman et al., 2018), predictions of tropical rainfall variability remain a challenge (Westra et al., 2014; Prakash et al., 2016). Stephens et al. (2010) demonstrated that the models predict too many rainy days in the tropics, which are in the lighter rain category. The challenges of tropical rainfall variability have also been demonstrated by Watson et al., 2017. The vagaries of the Indian monsoon every year affect the lifestyle of billions of people and the economy of the Indian sub-continent, modulating its Gross Domestic Product (GDP) (Gadgil and Gadgil, 2006). It is, therefore, of the utmost importance to improve the weather prediction skill in general and extreme precipitation events in particular. With the increase in computing power, the resolution of numerical weather prediction models has been increasing, and global models with a resolution of 1~7 km have become a reality (Majewski et al., 2002; Satoh et al., 2005; Miura et al., 2007; Staniforth and Thuburn, 2012; Li et al., 2015; Satoh et al., 2019; Wedi et al., 2020). The higher resolution of Numerical Weather Prediction (NWP) models has been found to produce a realistic rainfall variability across scales including diurnal variation, better Madden Julian Oscillation (MJO) variability and seasonal mean climate (Kinter et al., 2013; Rajendran and Kitoh, 2008; Skamarock et al., 2012; Molod et al., 2015; Crueger et al., 2018; Giorgetta et al., 2018). In India, operational NWP was initiated with a moderate resolution of T80 and then gradually enhanced to T382, T574 (Prasad et al., 2011, 2014, 2017), and very recently to T1534 (Mukhopadhyay et al., 2019). The advantage of using a higher resolution (T1534~12.5 km) as against the lower resolution T574 (~27 km) was found by enhancement of the model skill by 2 days (Rao et al., 2019). The National Centre for Environmental Prediction (NCEP) GFS model with 21 members has been used for probabilistic forecasts since June 2018 (Deshpande et al., 2021). The high-resolution GFS T1534 is found to enhance the skill of heavy rainfall events (Mukhopadhyay et al., 2019), tropical cyclones, and even block level prediction of rainfall (block is a sub-division of districts in India, typically of the size of the grid of GFS T1534). However, the skill of the GFS T1534 for the prediction of extremely heavy precipitation can still be improved, particularly over the orographic regions of India, such as the southern coastal state of Kerala, India (Mukhopadhyay et al., 2021).

The 12-km deterministic and the ensemble model based on the GFS show reasonably good skill in capturing the monsoon rainfall with 3 to 5 days lead time. The skill of the GFS forecast for the Indian monsoon has been reported by Mukhopadhyay et al. (2019), and the skill of tropical cyclones with the Global Ensemble Forecast System (GEFS) has also been reported by Deshpande et al. (2021) and Kanase et al. (2023). However, in a recent study, Mukhopadhyay et al. (2021) showed that three state-of-the-art ensemble forecast systems, namely the GEFS, the United Kingdom Meteorological Office (UKMO) based NCMRWF Ensemble Prediction System (NEPS) run by National Centre for Medium Range Weather Forecasting (NCMRWF) and the Integrated Forecasting System (IFS) by ECMWF struggled to capture the extremely heavy rainfall over Kerala state of India during August 2018 and August 2019 extremely heavy rainfall episode. This, in fact, brought up the limitation of the model in resolving the rainfall variability over the Indian region and, more importantly, over the orographic region. One of the limitations in resolving the regional variabilities of rainfall is the horizontal resolution

which does not allow the model to resolve the smaller scale processes. Therefore, a need was felt to enhance the horizontal resolution of the existing GFS-based forecasting system. As running a model close to the convection permitting model (at a resolution lesser than 10 km) is computationally too expensive in conventional linear reduced Gaussian grids, it was thought to build a weather model with a grid that has a variable resolution from the pole to the equator. In view of this, the GFS linear reduced Gaussian Grid at triangular truncation 1534 is replaced by an equivalent truncation of 1534 in a triangular cubic octahedral (Tco) grid. The equivalent model resolutions of the linear T1534 and the cubic Tco1543 grids are displayed in Fig. 1a. Indeed, as the linear grid has a roughly uniform grid point resolution of 12.5 km, the octahedral grid has a resolution of about 8 km in the Polar Regions and around 6 km in the tropical band. One of the prominent examples of the Global NWP model with the Tco grid is that of the European Centre for Medium-Range Weather Forecasts (ECMWF) model suites. The Tco grid provides several advantages (ECMWF Documentation Cy43r1, 2016) over that of the conventional reduced Gaussian linear grid (Fig. 1a), to name a few- significant reduction in computation cost, improved representation of orography, better filtering, and better conservation properties. These properties of Tco make it a better candidate, particularly for the utilization of high-performance computers (HPC).

To the best of our knowledge, this paper is the first attempt towards building a model close to a convection permitting global weather model in India with an emphasis on Indian monsoon rainfall variability. The details of the model development and the experiments conducted have been elaborated in Sect. 2. The model results are analysed in Sect. 3, and the conclusion of the study is summarized in Sect. 4.

2 Model, Data, and Methodology

This new grid, namely the Triangular Cubic Octahedral (Tco) grid, has been adopted to change the existing GFS (semi-lagrangian) Gaussian linear model system. In the spectral domain, dynamical fields are represented by the sum of spherical harmonics. The total wavenumber characterizes the spherical harmonics, and the associated wavelength is the ratio of the circumference of the Earth to the total wavenumber. The value of the maximum wavenumber (n_max) used to represent a field as the sum of spherical harmonics is also the spectral truncation of the model. In the case of both GFS and Tco, the value of n_max is 1534. For the same spectral truncation n_max, the number of latitude circles from the equator to the pole can vary depending on the choice of spectral transformation. For a linear grid, n_max=2N-1, and for a cubic grid, n_max=N-1. Therefore, for a linear Gaussian grid, the smallest wavelength is represented by only two grid points, as is the case with the GFS 1534 model. However, in the case of triangular truncation, the smallest wavelength is represented by four grid points (in the case of the Tco grid). In triangular truncation, for the same spectral truncation, the number of latitude circles is about double that of the linear truncation. For the GFS model, the horizontal resolution is ~12.5 km, and applying the cubic grid ensures that the horizontal resolution becomes ~6.5 km in the tropics (about half of the currently used model resolution) for the Tco grid. In the Tco grid, the number of latitude circles is 1535.

Once a particular choice of spectral truncation is made, the number of latitude circles becomes obvious. However, the number of longitude circles per latitude circle remains to be prescribed for creating the global grid structure. In a fully Gaussian grid, the number of longitude circles per latitude circle remains the same throughout the latitudes from the equator to the pole. Thus, the effective resolution near the poles becomes very high compared to the equatorial regions. This specific requirement demands too many computational resources and poses numerical instability problems. To overcome that, in the linear Gaussian grid, the number of latitude circles decreases in a certain way from the equator toward the pole to ensure almost the same zonal resolution. For the cubic octahedral grid, the number of longitude points per latitude circle is prescribed differently. The latitude circle closest to the pole consists of 20 longitude points, and the number of longitude points increases by 4 at each latitude circle, moving from poles towards the equator. The number of longitude points at the equator in the case of the Tco grid is given by Nx=20+1534*4=6156. Therefore, the zonal grid length=2pi*R/Nx~6.5 km. In the original reduced Gaussian grid, the number of longitude points per latitude remains fixed in different blocks of latitudes. The number of latitude points jumps from one block to another by a constant number. Unlike the linear reduced Gaussian grid, the horizontal resolution varies more smoothly with latitudes in Tco. The Collignon projection of a sphere obtains this configuration onto an octahedron. In the current study, the Tco grid at truncation wavenumber of 1534 is being used. This new version of the model is mentioned as HGFM (High-resolution Global Forecast Model Version 1) throughout the manuscript. Fig. 1a and Fig. 1b depict the variation of grid resolution with latitude in the GFS (SL) and HGFM (Tco).

Before testing the HGFM with complete physics (see Table 1 for a description of physics used in both versions of the model), we have developed a version of HGFM with only a dynamical core following the approach of Held and Suarez (1994), referred to as HS94. The HS94 was run to check the stability of the Tco grid framework. Surface boundary conditions for the Tco grid were meticulously prepared to ensure the accuracy of grid-point representation. Moreover, the HGFM (Tco1534) has been developed with complete physics and incorporates essential boundary conditions, including global topography, global land-use-land-cover, etc. The HGFM at Tco1534 truncation is depicted over the globe in Fig. 1. The model has been run daily for ten days forecast at IITM Pratyush HPC system. To understand the computational efficiency of the Tco model, the time taken for one day forecast is compared for GFS 1534 and HGFM model (Tco 765 in this case) (see Fig. 1c). A comparison between GFS 1534 and Tco 765 is made because both models have nearly the same number of grid points. It is evident that Tco 765 significantly saves the runtime in dynamical core and total time as well. Moreover, the Tco model is in general more scalable for higher number of cores (not shown). The model has been running since 2022, and here, the analyses for the summer monsoon season of June, July, August, and September (JJAS) 2022 are being presented. A detailed analysis of the model run is discussed in the results section. Apart from the monsoon season (JJAS 2022), a few case studies are also discussed.

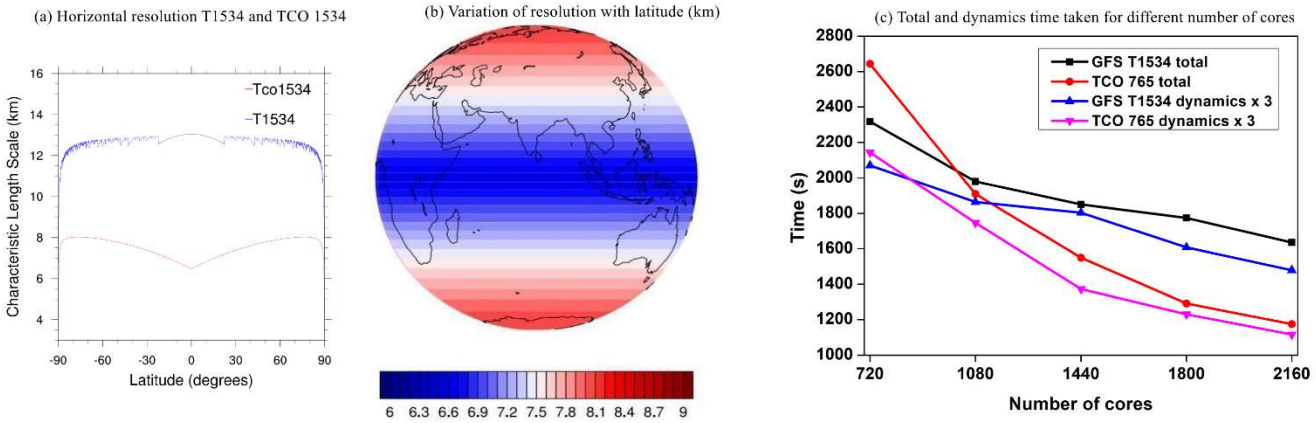

151

152 **Figure 1. Variation of grid length with latitude in GFS (blue) and Tco (red) (a), depiction of grid resolution over the globe in Tco**
153 **grid (b), total and dynamics time taken for different number of cores (c). Time taken by GFS and HGFM for one day forecast**
154 **(Left vertical axis is total time taken and model dynamics time multiplied by 3).**

155 To verify the model forecast, the daily observed gridded rainfall data from the Integrated Multi-satellite Retrievals for GPM
156 (IMERG) version 06B (Huffman et al., 2019) rainfall data at 0.1◦ × 0.1◦ (10 km) horizontal resolution is utilized for the year
157 of 2022 for JJAS season. Additionally, for the validation of a heavy rainfall event over India, gridded rainfall data from the
158 India Meteorological Department (IMD) at 25 km resolution is used. The IMD rainfall data are a merged product of gridded
159 rain gauge observations and GPM satellite-estimated rainfall over the Indian Summer Monsoon (ISM) region (Mitra et al.,
160 2014). Further, the reanalysis-based parameters from the fifth generation of ECMWF atmospheric reanalyses (ERA5)
161 products (Hersbach and Dee, 2016) at 25 km horizontal resolution are utilized during JJAS season of the year 2022.

162 **Table 1. Details of domain configuration and physics options used in HGFM.**

Physics	Description
Radiation	Rapid Radiative Transfer Model (RRTM) for both Shortwave and Longwave (Iacono et al., 2000; Clough et al., 2005) with Monte Carlo Independent Column Approximation (McICA)
Microphysics	Formulated grid-scale condensation and precipitation (Sundqvist et al., 1989; Zhao and Carr, 1997)
Convection	Aerosol aware and Mass flux based Simplified Arakawa-Schubert (SAS) shallow convection (Pan and Wu, 1995; Han and Pan, 2011; Arakawa and Wu, 2013; Han et al., 2017)
Planetary Boundary Layer (PBL)	Hybrid Eddy-Diffusivity Mass Flux vertical turbulent mixing scheme (Han and Pan, 2011; Han et al., 2016)
Gravity Wave Drag (GWD)	Mountain blocking (Alpert et al., 1988; Kim and Arakawa, 1995; Lott and Miller, 1997) and stationary convective-forced GWD (Chun and Baik, 1998)

163

3 Results and Discussions

3.1 200 hPa Kinetic Energy Spectra

Before going into the details of model validation, the first metric to evaluate the model fidelity is to validate the Kinetic Energy (KE) spectra of 200 hPa wind. The KE spectra provide information about the distribution of kinetic energy across scales. A close resemblance between observed /reanalysis-based spectra and spectra produced by the model gives confidence about the accuracy of overall model configuration. The kinetic energy (KE) spectrum in the upper troposphere exhibits two clearly defined power-law patterns. From observational studies, it is established that at large scale, rotational modes prevail (k^{-3}), while at mesoscales, divergent modes are dominant ($k^{-5/3}$) (Nastrom and Gage, 1985). Figure 2 shows the KE spectra of 200 hPa wind simulated by HGFM and GFS T1534. The KE spectra for the forecast up to 3 days lead time have been compared with ERA5 data. While both the models reasonably capture $k^{-5/3}$ behaviour of the mesoscale at the higher wavenumber, HGFM appears to capture the k^{-3} behaviour of the large scale at the lower wavenumber closer to observation. It is observed that beyond wavenumber 10^{-4} there is a slight departure of the spectra from observation, especially for HGFM. However, the regions of interest in KE spectra are the k^{-3} dependence for the large scale and a less steep, $k^{-5/3}$ dependence for the mesoscale. The tail of the spectra at higher wavenumbers typically has less energy due to the dissipation of kinetic energy with an increase of wavenumber. However, models tend to dissipate the energy at higher wavenumbers at a much faster rate depending on the damping used in the model (Skamarock, 2004). To keep the spectra realistic, a common practice is to reduce the damping, which may increase the energy at higher wavenumbers, as observed in this case for HGFM. However, this will not have much impact on our analysis as these are the small-scale features. The KE spectra indicate that the overall configuration of both versions of the model is robust. Therefore, we now turn our attention towards verification of convective available potential energy and rainfall simulations, the most desirable parameters in model forecasts.

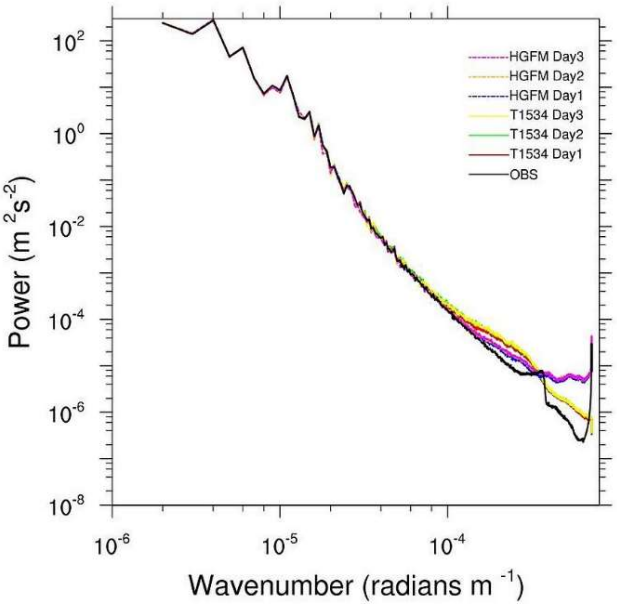

185

186 **Figure 2. Kinetic energy spectra of 200 hPa wind for observation and different lead times of GFS T1534 and HGFM.**

187 **3.2 Quasi-equilibrium in models**

188 Both model versions are run at high-resolutions, close to convection-permitting models' resolution. However, in this case, a
189 scale-aware convection scheme is used to parameterize deep convection in the model. From observational studies, it has
190 been established that tropical atmosphere deviates significantly from the convective-quasi equilibrium (e.g., Zhang, 2003).
191 The convective quasi-equilibrium (CQE) is the fundamental approach used in most models for parameterization of deep
192 convection (Arakawa and Schubert, 1974). To understand the extent to which both model versions obey CQE, we adopted
193 the methodology suggested by Kumar et al. (2022). The absolute value of changes in Convective Available Potential Energy
194 (CAPE) at daily timescales is analysed from GFS T1534 and HGFM models for the year 2022 during JJAS and compared
195 with the ERA-5 data (Figure not shown). Notable changes were observed in the daily dCAPE values between GFS T1534
196 and HGFM compared to ERA-5. The daily dCAPE values from ERA-5 data match better with the HGFM than GFS T1534
197 for day 1 and day 3 lead times. The difference of dCAPE between ERA-5 and models is presented for day-1 and day-3 lead
198 time forecasts (Fig. 3). The dCAPE difference quantified from ERA-5 with GFS T1534 were –49.0570 (J/kg/day) and –
199 47.3799 (J/kg/day) for day1 and day 3 lead times, respectively. Similarly, with HGFM, the values were –49.1278 (J/kg/day)
200 and –43.7668 (J/kg/day) for day 1 and day 3 lead times, respectively.

201

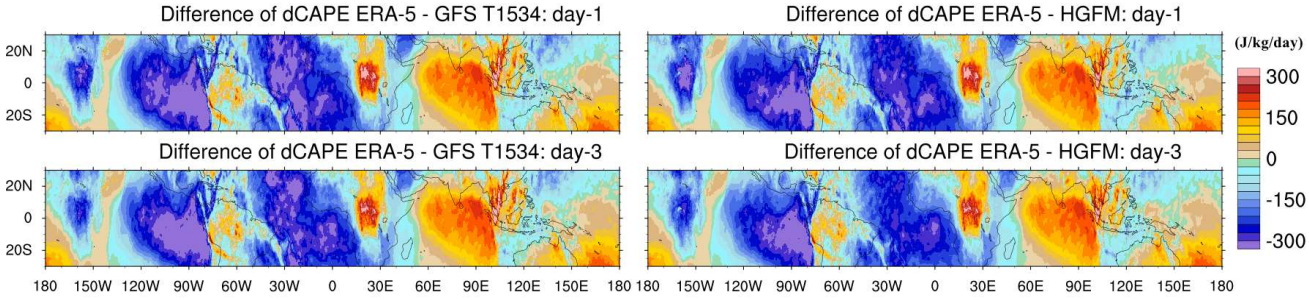

Figure 3. The difference of dCAPE between ERA-5 and GFS T1534 for day-1 and day-3 (left panels), and between ERA-5 and HGFM for day-1 and day-3 (right panels).

3.3 Analysis of Global Precipitation

The global precipitation bias of GFS (left panel of Fig. 4 and HGFM (right panel) with respect to Integrated Multi-satellite Retrievals for GPM (IMERG) data, with day 1, day 3, and day 5 lead times, is shown in Fig. 4. Both the models broadly show a similar rainfall bias over the global land and global ocean. However, there are some subtle differences. The day 1 forecast (Fig. 4a) of GFS shows a wet bias over the equatorial eastern Pacific extending up to the tropical western Pacific. On the other hand, the HGFM on day 1 lead (Fig. 4d) also shows a wet bias mostly confined over the tropical eastern Pacific and a slight negative bias over the western Pacific. For HGFM, the positive bias of rainfall over the tropical ocean appears to be mainly over the eastern Pacific, while that of GFS appears to extend from the eastern pacific towards the central and west Pacific for all the lead times. The eastern Pacific precipitation overestimation could be due to improper representation of shallow convection over the region. Raymond (2017) highlighted the complex nature of SST and associated cloudiness and convection over the region. Apart from the oceanic region, the major global land regions (central African Continent, Maritime continent, Indian summer monsoon region, northern part of South America) show a negative bias in both the models at different lead times (Fig. 4) which is likely related to the model's physical parameterizations.

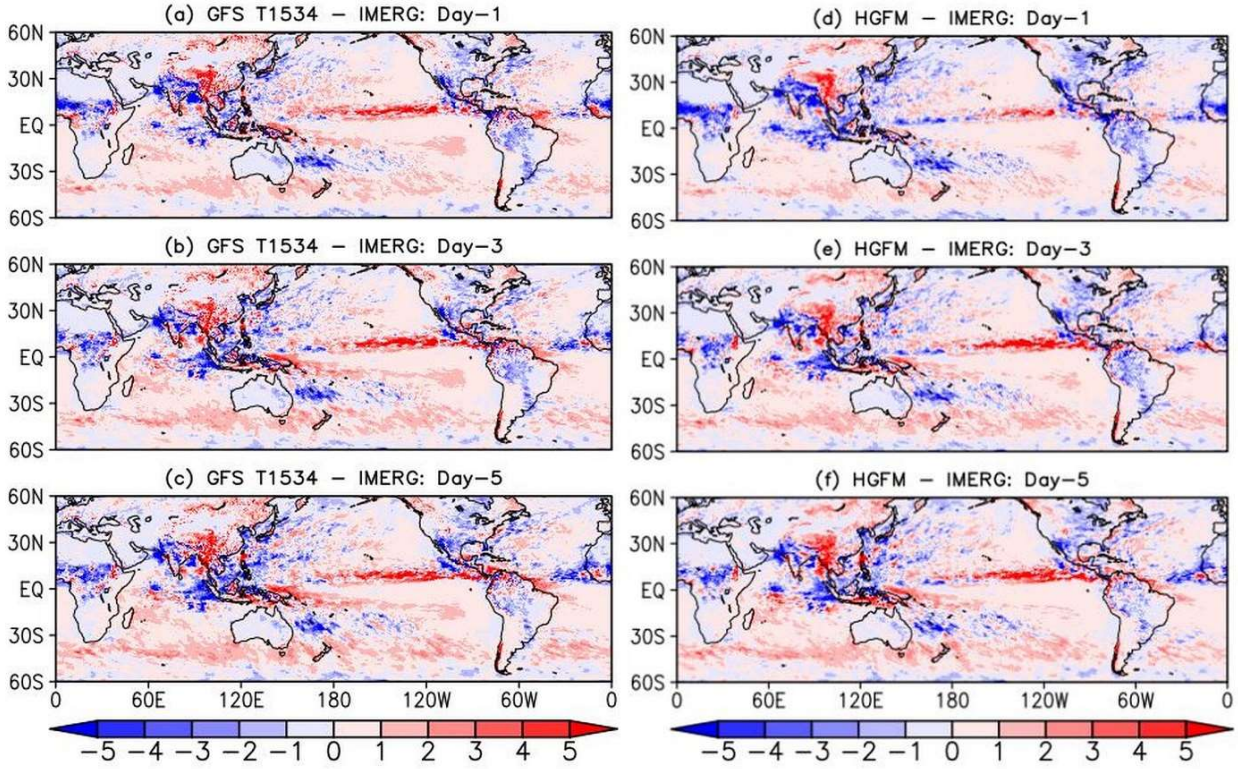

Figure 4. Global JJAS precipitation bias (cm/day) of GFS T1534 (left panel) with respect to IMERG for (a) day-1, (b) day-3 and (c) day-5 lead time. Right column (d-f) indicates similar plots but for HGFM.

3.4 Indian summer monsoon precipitation and related features

While Fig. 4 depicted the precipitation bias over the global domain, it will be interesting to investigate the model forecast performance over the complex orographic region over the Indian domain, the region of our utmost interest. As mentioned earlier, one of the major advantages of using a Tco grid is that it better represents orography. Therefore, it is imperative to investigate the forecast skill of the high-resolution HGFM model over the mountainous Himalayan foothills, adjoining northeast India, and Western Ghats (WGs) region (shown in Fig. 5 and 6 respectively). The GFS T1534 model forecasts indicate spurious rainfall activity over the Himalayan foothills and northeast India region for all lead times (Fig. 5b-d). On contrary, the HGFM model with finer horizontal resolution largely resolves the spurious rainfall over the region, as shown in Fig. 5e-g. The Gibbs waves are largely suppressed over the mountainous terrains in HGFM compared to GFS T1534. Similarly, the precipitation distribution over the WGs region shows considerable overestimation in GFS T1534 for all lead times (Fig. 6b-d). On the other hand, the magnitude of overestimation is decreased considerably in HGFM forecasts, as depicted in Fig. 6e-g. Thus, the above analysis highlights the fact that HGFM shows its potential in predicting realistic rainfall distribution over the orographic regions.

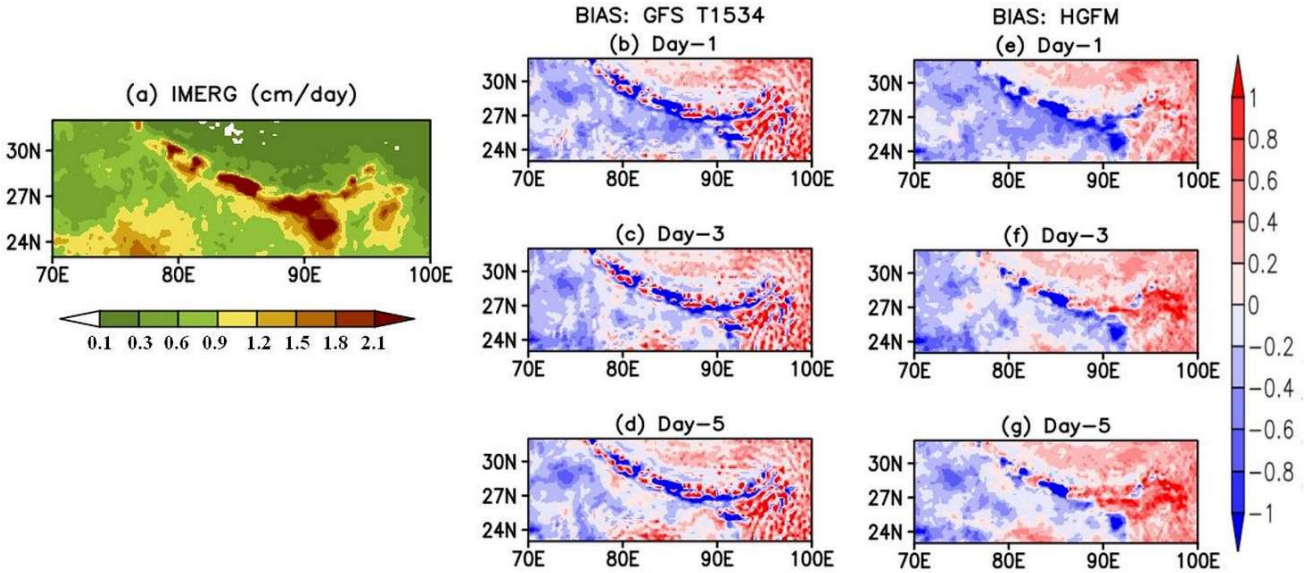

236

237 **Figure 5. Comparison of JJAS mean precipitation (cm/day) and Bias in IMERG data (cm/day) (a) with GFS T1534 (b, c, d) and**
238 **TCO 1534 (e, f, g) during 2022 over Himalayan foothills and Northeast India for day-1 day-3 and day-5 lead time.**

239

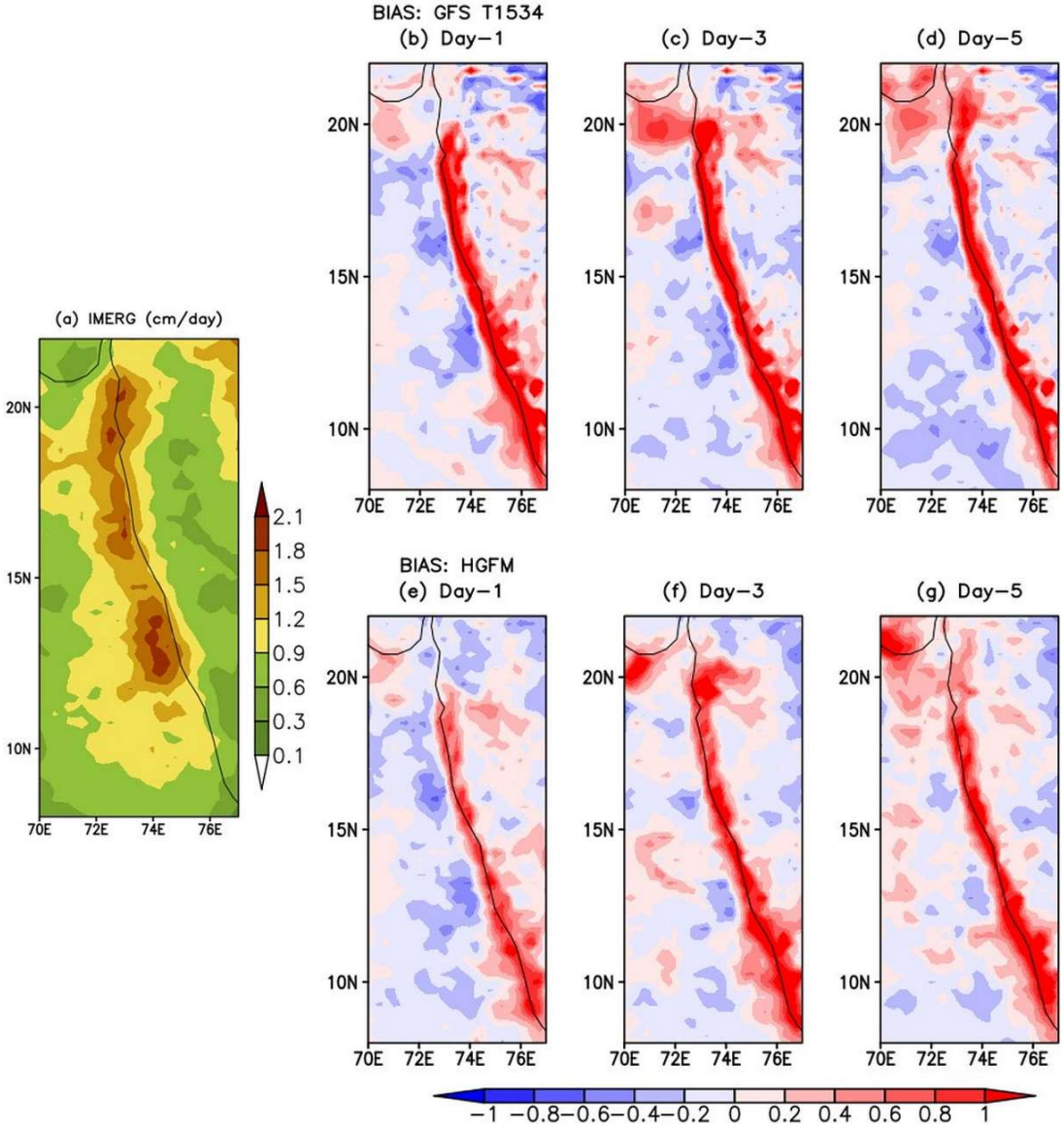

Figure 6. Comparison of JJAS mean precipitation (cm/day) and Bias in IMERG data (cm/day) (a) with GFS T1534 (b, c, d) and TCO 1534 (e, f, g) during 2022 over Western Ghats region for day-1 day-3 and day-5 lead time.

One of the prominent features of ISM is the vertical shear of zonal wind. Previous studies (Jiang et al., 2004; Abhik et al., 2013) demonstrated that the vertical easterly wind shear plays a crucial role in inducing baroclinic vorticity ahead of the northward propagation of summer intra-seasonal oscillation. To assess the model forecast skill in predicting realistic easterly wind shear (difference between zonal wind at 200 and 850 hPa) during the summer monsoon season of 2022, the vertical wind shear calculated and is represented in Fig. 7a and 7b for GFS T1534 and HGFM, respectively, over the ISM region. Figure 7a indicates slightly weaker easterly shear in GFS T1534 compared to ERA5 around 10° N and 0°-15° S for all lead

times. On the contrary, the HGFM predicts more realistic easterly wind shear over the above regions, as shown in the Fig. 7b. It is noticeable that both models overestimate the magnitude of easterly shear around 20^{o} N for Day-3 and Day-5 lead times.

Another key feature of tropical precipitation is almost equipartition of rainfall into convective and stratiform rain. Therefore, it is important to investigate whether the relative improvement in the precipitation distribution over the ISM region in HGFM forecasts is contributed by improved convective and large-scale precipitation. The model forecasted convective and large-scale rainfall ratios are shown in Fig. 7c and 7d respectively. It is noteworthy that the large-scale or stratiform rainfall plays an important role in the propagation and maintenance of the tropical intraseasonal convection, associated with its top-heavy heating profile (Fu and Wang, 2004; Chattopadhyay et al., 2009; Deng et al., 2015). The heating profile associated with stratiform rain also helps in large-scale organization of convection (see, for example, Choudhary and Krishnan, 2011, Kumar et al., 2017). The contribution of convective rainfall to the total rainfall appears to be more than 80 % in GFS T1534 forecasts for all lead times (Fig. 7c). A similar overestimation of convective rainfall in GFS T1534 is reported by Ganai et al. (2021). The observed convective (large-scale) rainfall ratio is around 55 % (45 %), as shown in Abhik et al. (2017). The HGFM forecast shows relative improvement in predicting convective and large-scale rainfall ratios compared to GFS T1534 (Fig. 7c and 7d). The decrease (increase) in convective (large-scale) rainfall contribution to total rain is noted in HGFM forecast. The finer horizontal resolution in HGFM possibly allows for a more accurate representation of deep convection due to scale-aware representation.

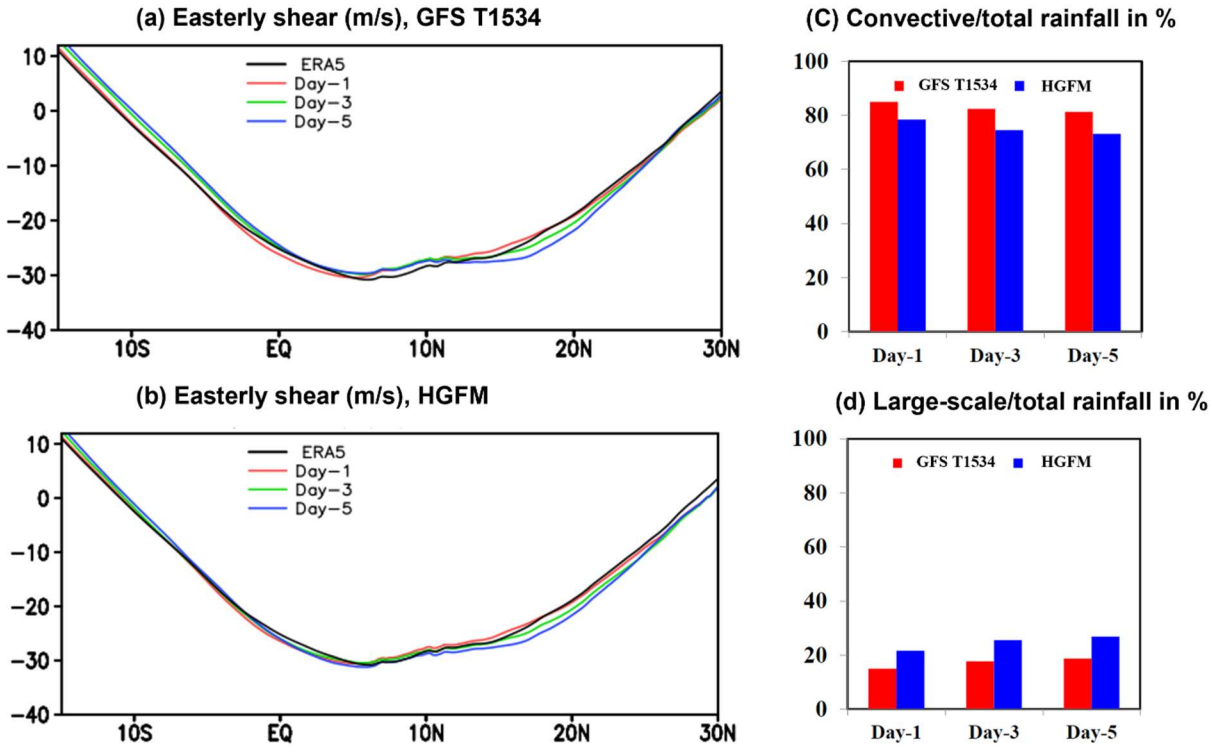

Figure 7. Comparison of easterly shear (m/s) from ERA-5 with GFS T1534 (a) and HGFM (b) along with convective/total rainfall (c) and large scale/total rainfall (d) between GFS T1534 and HGFM during JJAS 2022 for day-1 day-3 and day-5 lead time.

To attain further clarity about the model precipitation and moist convective processes, the vertical profile of relative humidity as a function of rain rate is analyzed for JJAS of 2022 over the ISM region (60° E-100° E, 10° S-30° N). The bias analysis suggests that GFS T1534 has systematically underestimated the lower-level moisture for all lead times (Fig. 8b). This is consistent with the findings of Mukhopadhyay et al. (2019), and Ganai et al. (2021), who reported a similar underestimation of lower-level moisture over the ISM region in GFS T1534 forecast. In contrast, the HGFM shows relative improvement in the lower-level moisture distribution, as depicted in Fig. 4c for all lead times. The enhancement of the lower-level moisture is noticeable compared to the GFS T1534 forecast. However, the upper troposphere is too moist for both model forecasts and requires further improvement.

It is observed that the overall statistics of monsoon rainfall and related convective processes have significantly improved in the HGFM model. In the next section, a case of heavy rainfall is discussed, followed by the analysis of recent tropical cyclone forecasts.

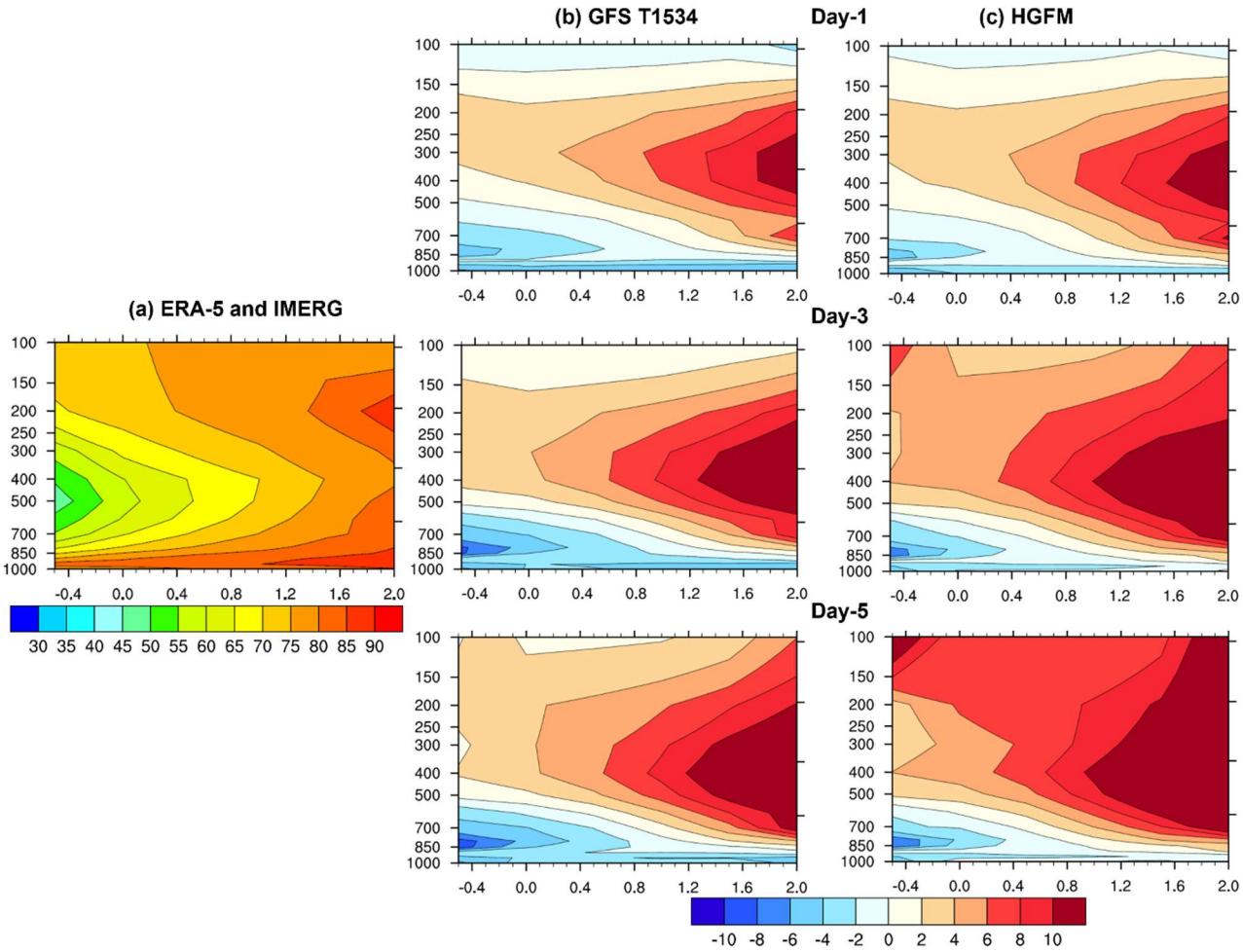

Figure 8. Comparison of Relative humidity (%, bias in shaded) vs rain rate (mm/day) over ISM region (60° E-100° E, 10° S-30° N) during JJAS-2022 from ERA-5 and IMERG (a) with GFS T1534 (b) and HGFM (c) during JJAS 2022 for day-1 day-3 and day-5 lead time.

3.5 Evaluation of Heavy Rainfall event

A very heavy rainfall event occurred on 22 August 2022 over central India. This event was well captured by both GFS T1534 and HGFM models as compared to the observed rain from IMD-GPM (shown in Fig. 9). Both HGFM (Fig. 9a, b, c) and GFS T1534 (Fig. 9d, e, f) models simulated the heavy rainfall signature compared to IMD-GPM (Fig. 9g) on day 1 and day 3 forecasts. However, a significant difference was noted in rainfall intensity and spatial distribution at longer lead times (day 5) in HGFM and GFS T1534. Both the models underestimated rainfall compared to observations. Nevertheless, the HGFM captures the signal of heavy rainfall occurrence even at day 5 lead time, which is almost negligible in the GFS T1534 forecast. Further, the precipitation probability distribution function (PDF) is analyzed (figure not shown) for the JJAS 2022

monsoon. It is found that the HGFM shows a better PDF in the very heavy (11.56-20.45 cm/day) and extreme (>20.45 cm/day) rainfall categories compared to GFS T1534.

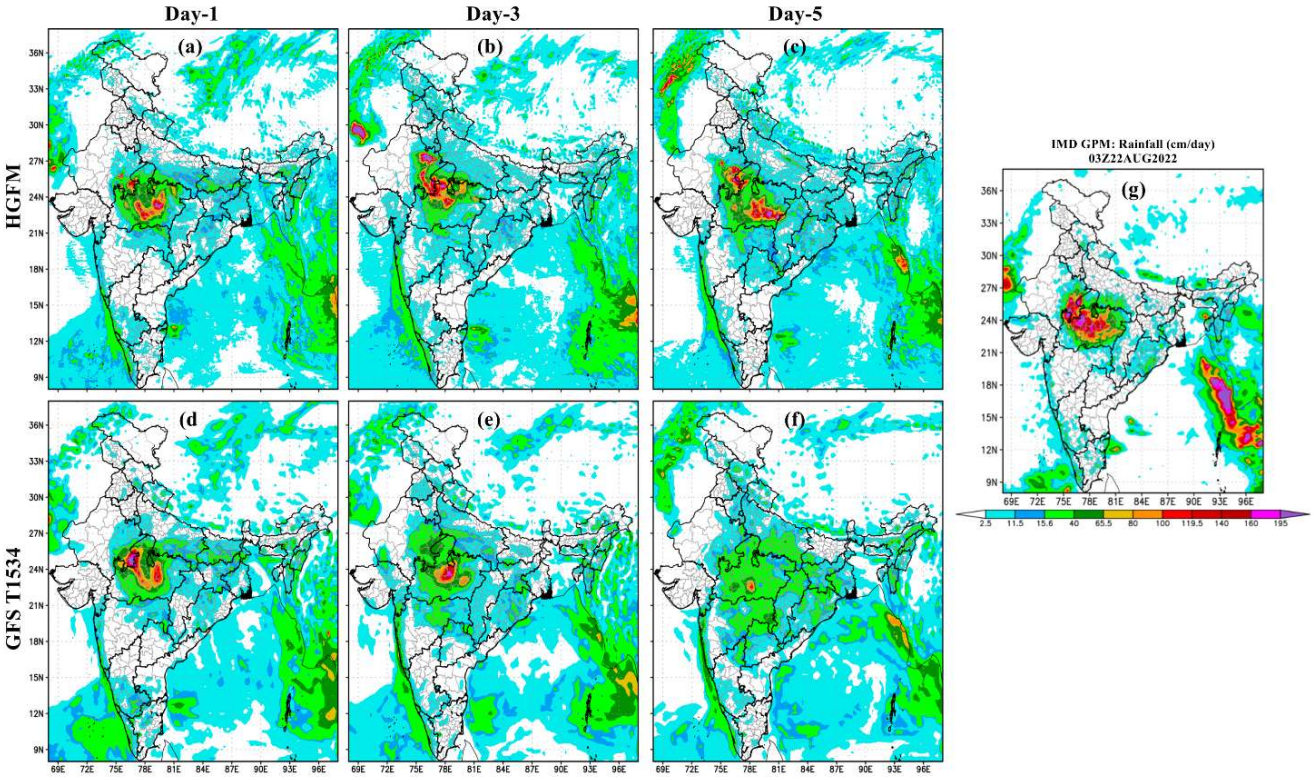

Figure 9. Comparison of heavy rainfall event on 22 August 2022 with HGFM (a, b, c), GFS T1534 (d, e, f) for day-1, day-3, and day-5 lead times with IMD GPM (g) rainfall.

3.5 Evaluation of Tropical Cyclone Forecast

A Total of eight named tropical cyclones occurred during 2022 and 2023 (RSMC 2022, RSMC 2023), which are considered in the present study. Out of these eight cases, two cyclones formed over the Arabian Sea and six cyclones over the Bay of Bengal (BOB). The best track data of track, intensity, and landfall is obtained from IMD and referred to as observations henceforth in the text. Figure 10 shows the observed tracks (Fig. 10a) and observed intensity in terms of the Maximum Sustained Wind Speed (MSW Fig. 10b) of the cyclones. The cyclones in the present study have different tracks and various ranges of severity in terms of intensity over both basins.

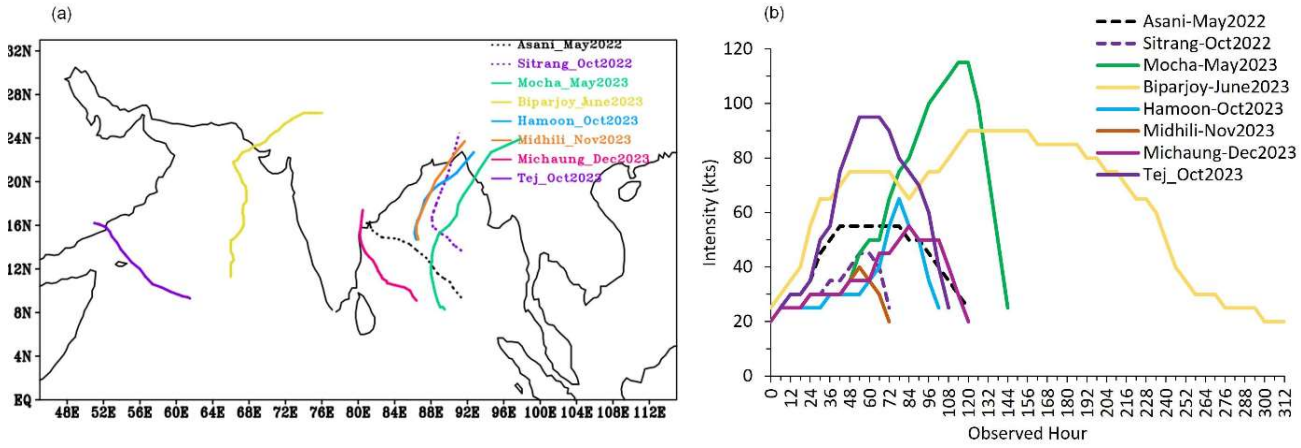

Figure 10. a) Observed tracks of the cyclones b) Observed Intensity in terms of Maximum Sustained Wind Speed (kts) during year 2022-2023.

3.5.1 Verification of GFS T1534 and HGFM Forecast for tropical cyclone cases during 2022 and 2023

For this verification, the lifetime of the cyclone is considered starting from the depression stage untill landfall, as per the observation. The total sample includes a minimum of four and a maximum ten initial conditions for typical cases, depending on the lifespan of the case. The errors calculated here are averaged for each forecast hour within the sample.

The Root Mean Square Error (RMSE) for track and intensity is shown in Fig. 11a and b, respectively. Initially, upto 4 days, GFS T1534 and HGFM perform equally well, but considerable improvement with HGFM is noted after 4 days in both track and intensity forecasts. Figure 11c-d depicts the average track error and average intensity errors for all the cyclones. The average track errors, as well as average intensity errors, are reduced drastically in HGFM with longer lead hours (4 days or more). Average track errors (average intensity errors) are ~300 km (~20 kts) with 7 days leads in HGFM. The average landfall errors (both position and time) are also evaluated with IMD observations and are shown in Fig. 12. With 4 days lead, average landfall position errors are ~200 km in HGFM and about 250 km for GFS T1534. Overall, the landfall position errors are less for HGFM. Remarkable improvements are seen in the average landfall time errors in HGFM throughout the life cycle of cyclones. Overall, the track and intensity forecast are improved with HGFM for longer lead hours (~4 days or more), which is an added advantage for the early warning and mitigation purposes. Here, one of the cyclone cases (cyclone Biparjoy) is discussed in detail.

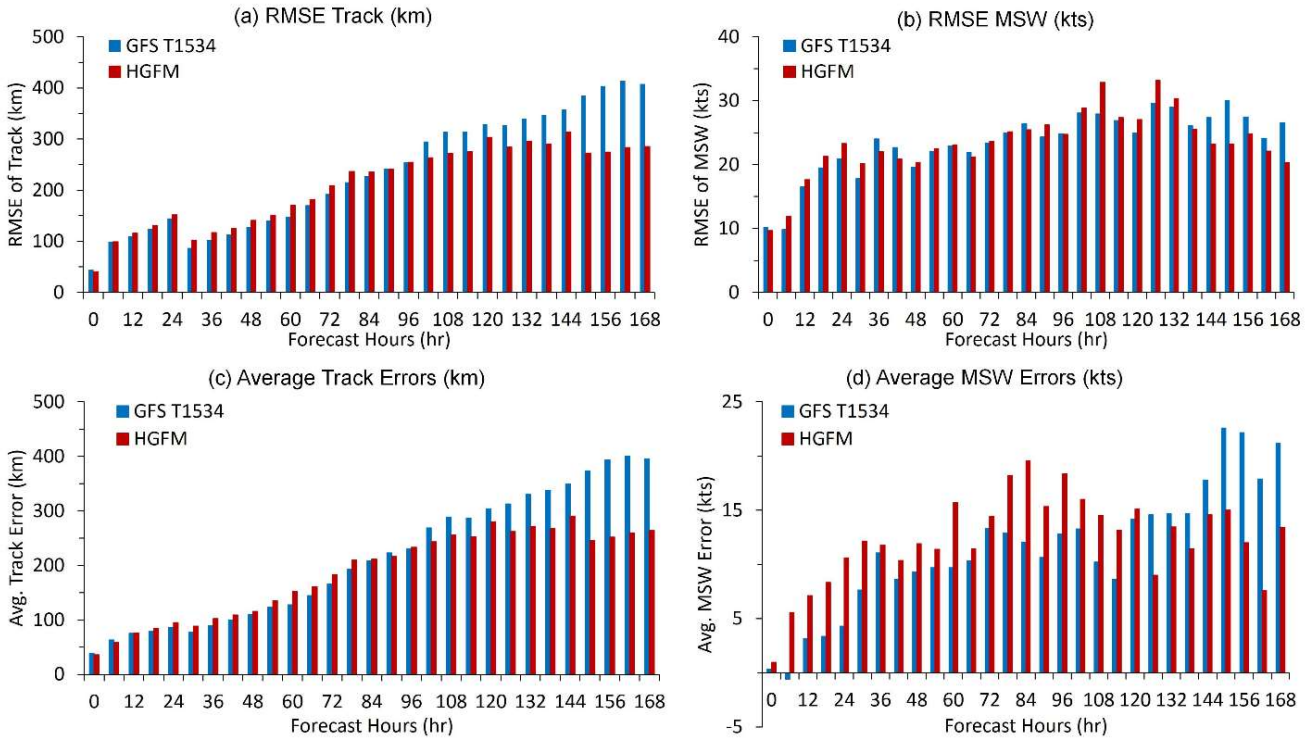

328

329 **Figure 11. a) RMSE of Track in km b) RMSE of MSW in kts c) Average Track error (km) d) Average Intensity Errors (kts).**

330

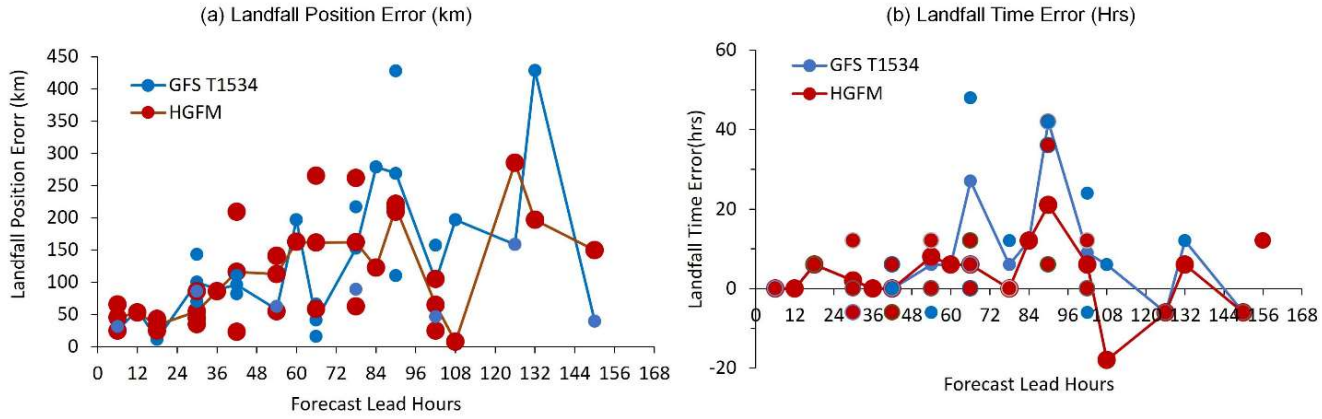

331

332 **Figure 12. a) Average Landfall position errors in km b) Average Landfall time Errors in hours. The continuous lines represent the**
333 **average errors for GFS T1534 (Blue) and HGFM (Red). The different sizes of the dots are for making the overlapped points**
334 **visible.**

3.5.2 A case study - Cyclone Biparjoy

During the monsoon onset of the 2023 season, tropical cyclone Biparjoy evolved in the Arabian Sea and hit the north-western state of Gujarat, India. The cyclone Biparjoy lasted for quite a long-time during 6-19 June 2023. As seen in figure 13a, it moved almost parallel to the Indian west coast and eventually recurved to make landfall over the northern part of Gujarat and adjoining Pakistan. It underwent rapid intensification during its genesis and growth stages on 6 and 7 June. This case was particularly challenging for prediction due to combination of recurving track, rapid intensification, slow movement, and a long lifespan. The HGFM and GFS T1534 track and intensity forecast of TC Biparjoy, based on 6 June (day of genesis) initial condition, are shown in Fig. 13 a and b, along with the best track data from IMD. It is evident that the HGFM predicts a track much closer to the observation compared to GFS T1534. Particularly, the recurvature is better captured by HGFM at about 6-7 days lead time. Both models overestimated the intensity untill 120 hrs of forecast,after which they indicated the dissipation phase.

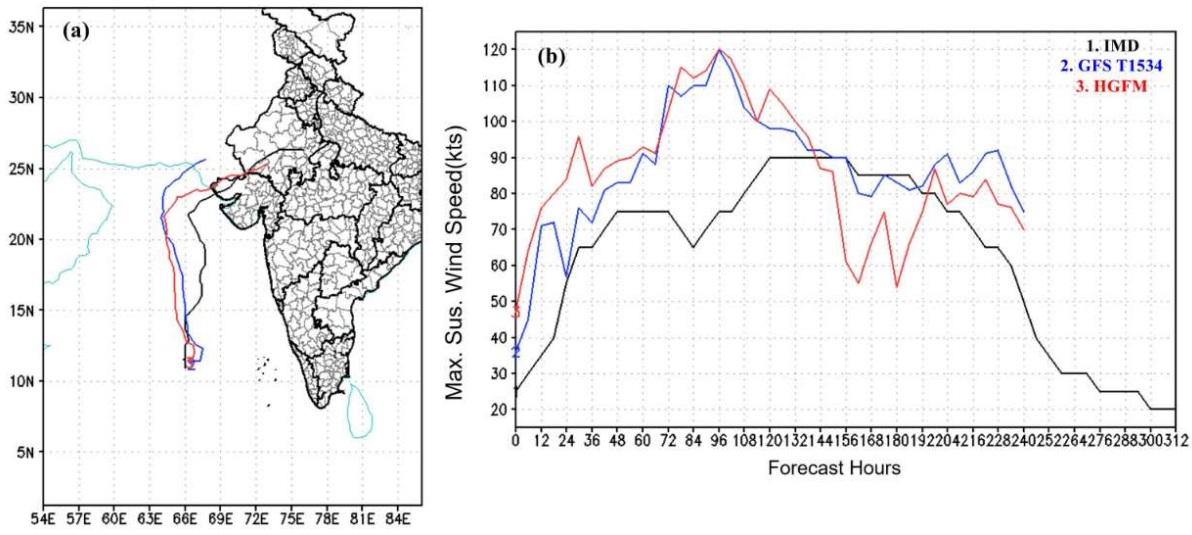

Figure 13. (a) track and (b) intensity variation forecast by GFS T1534, HGFM and as reported by IMD for the case of oTropical cyclone Biparjoy over Arabian Sea based on 6 June 2023 initial condition.

To assess the robustness of the performance, verification is carried out for this particular case considering forecasts from all the initial conditions (from 6 June 00UTC to 15 June 00UTC, initialized at 24-hours interval). A comparative analysis of landfall position and landfall time errors for HGFM and GFS T1534, with respect to the data reported by IMD, is presented in Table 2. It is evident that the landfall position error of the cyclone has been significantly improved by HGFM forecast,

though the landfall time error appears to be almost equivalent as compared to GFS T1534. Further, the average track and intensity errors (obtained from a total of 10 initial conditions) are depicted in Fig. 14a and 14b. It is evident that HGFM consistently produces accurate predictions of track and intensity with lesser errors at longer lead times, while the errors for shorter lead times are more or less the same.

Table 2. Landfall position (km) and landfall time (hr) errors for the forecasts started with different initial conditions. -ve (+ve) sign indicates early (late) landfall with respect to observed landfall time. The bold numbers indicates the significant improvement in the landfall position errors with HGFM.

Forecast Hours from Observed landfall (Hr)	Initial Condition	Landfall Position Error (km)		Landfall Time Error (Hr)	
		GFS T1534	HGFM	GFS T1534	HGFM
228	2023060600	298	**57**	0	-30
204	2023060700	No Landfall			
180	2023060800	616	**201**	0	0
156	2023060900	349	**197**	12	12
132	2023061000	428	**197**	12	6
108	2023061100	197	**7**	6	-18
84	2023061200	279	**123**	12	12
60	2023061300	197	**163**	6	6
36	2023061400	89	**86**	0	0
12	2023061500	57	**53**	0	0

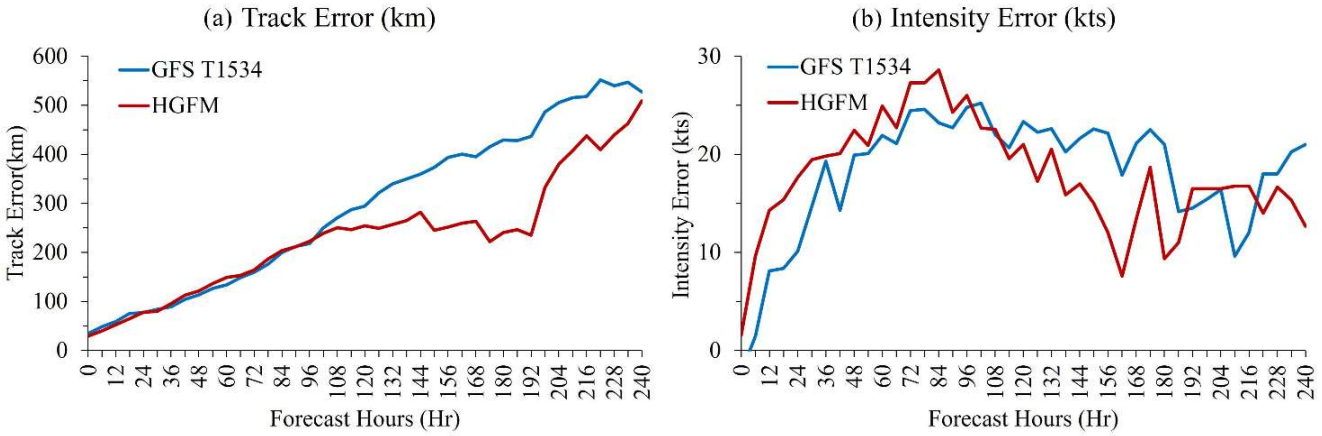

Figure 14. a) Average track error and b) average intensity error for the tropical cyclone Biparjoy over Arabian Sea.

4 Conclusions

For the first time, a version of the GFS model utilizing a new grid structure, the triangular cubic octahedral (Tco) grid, has been developed and is being run on an experimental basis for short to medium-range weather prediction over the Indian region, designated as IITM High resolution Global Forecast Model (HGFM). The Tco grid provides a higher resolution over the tropics, enabling the model to achieve a 6.5 km horizontal resolution near the tropics. This higher resolution represents a substantial leap from the existing Gaussian linear GFS T1534 which maintains a resolution of 12.5 km across the globe. The KE spectra of 200 hPa zonal wind have also revealed reasonable power by both the models with HGFM showing marginally better power in the Kolmogorov region, indicating the fidelity of the model structure.

It is worth mentioning that the present dynamical core, using the cubic octahedral grid, has been implemented in ECMWF weather forecast model since 2016 (Malardel et al., 2016). This has led to a significant increase in forecast accuracy and computational efficiency in the ECMWF model. In the present study, it is found that this dynamical core in the GFS T1534 has improved the orographic rainfall and reduces the Gibbs noise over the mountainous regions, in addition to improved precipitation skill over the Indian landmass region. The June-September monsoon rainfall and a case study of heavy rainfall have been analyzed in detail. The newly developed HGFM shows significantly better skill, particularly in the longer lead and for heavier rain categories. Rainfall biases over the entire globe appear broadly similar between HGFM and GFS T1534. A case of heavy rainfall in and around central India during the monsoon season has been analysed, where validation shows a significant gain in forecast lead time by HGFM compared to GFS T1534. The HGFM captures the rainfall signature at 5 days lead time, when there is hardly any indication in the GFS T1534 model forecast.

Several cases of tropical cyclones during 2022 and 2023 were analysed, indicating better performance of HGFM compared to GFS T1534 in predicting tracks and intensity. A detailed evaluation of tropical cyclone Biparjoy, based on IMD observation, reveals that the HGFM model provides better accuracy in cyclone position across almost all lead times (Table

2). Additionally, the average track error for HGFM is significantly lower than GFS T1534 at longer lead times. However, the average track and intensity errors for both the models are found to be equivalent. This paper highlights the initial results of the newly developed HGFM model and its skill as compared to the operational GFS T1534 model. Subsequently more analyses for many events will be carried out and the model will be made operational for weather forecasts over India. The current setup of the HGFM model uses the same physics as the GFS model. However, the HGFM model would require some parameter tuning to optimize and enchance the performance of the model and its fidelity. The future work will be focused on detailed validation of model simulations with optimal set of physical parameterizations.

Code and Data Availability

The model simulated data used for HGFM and GFS T1534 in the study are available at "TCO model data" by R Phani Murali Krishna, Kumar Siddharth, Athipatta Gopinathan Prajeesh, Malay Ganai, B. Revanth Reddy, Kumar Roy and Parthasarathi Mukhopadhyay, DOI: https://doi.org/10.5281/zenodo.12569807. The model code is available at "GFS TCO Model code" by R Phani Murali Krishna, Kumar Siddharth, Athipatta Gopinathan Prajeesh, Parthasarathi Mukhopadhyay. DOI: https://doi.org/10.5281/zenodo.12526400

Author Contributions

RPMK, SK, AGP and PM conceptualised the problem and made necessary changes/modification development of code for Tco and wrote the major part of the Introduction, data, methodology and over all sequences. PB and NW helped during formulation of the Tco grid in GFS and helped in improving the manuscript writing. KR, MG, ST, BRR and TG made all the forecast analysis of monsoon parameters and wrote the respective portion on analyses. RK, MD and SS made the analysis related to cyclone forecast by HGFM model and wrote the section on the cyclone forecast analysis and BRR made the dCAPE analysis and extracted the post processed variables for the analysis.

Competing interests

The authors declare that they have no conflict of interest.

Disclaimer

Acknowledgments

IITM is fully funded by the Ministry of Earth Sciences, Government of India. We would like to thank ECMWF for their support during the model development and for providing the ERA5 data set. We thank NCMRWF for providing the GFS initial conditions used for conducting simulations. We acknowledge Pratyush High Performance Computing at IITM, Pune for providing the computing facility to carry out the simulations. We thank Mr. Vaishak for helping in archiving the data in ARDC server. Authors thank Secretary Ministry of Earth Sciences, Government of India and Director, IITM for support and facilities provided for this study. We thank IMD for providing the IMD-GPM rainfall and cyclone best track data.

461 **References**

462 Abhik, S., Halder, M., Mukhopadhyay, P., Jiang, X., and Goswami, B.N.: A possible new mechanism for northward
463 propagation of boreal summer intraseasonal oscillations based on TRMM and MERRA reanalysis, Clim. Dyn., 40, 1611-
464 1624, https://doi.org/10.1007/s00382-012-1425-x, 2013.

465 Abhik, S., Krishna, R.P.M., Mahakur, M., Ganai, M., Mukhopadhyay, P., and Dudhia, J.: Revised cloud processes to
466 improve the mean and intraseasonal variability of Indian summer monsoon in climate forecast system: Part 1, J. Adv.
467 Model. Earth. Syst., 9(2), 1002-1029, https://doi.org/10.1002/2016MS000819, 2017.

468 Alpert, J.C., Kanamitsu, M., Caplan, P.M., Sela, J.G., White, G.H., and Kalnay, E.: Mountain induced gravity wave drag
469 parameterization in the NMC medium-range forecast model. In Conference on Numerical Weather Prediction, Baltimore,
470 MD, 8th, 726-733, 1988.

471 Arakawa, A. and Schubert, W.H.: Interaction of a cumulus cloud ensemble with the large-scale environment, Part I, J.
472 Atmos. Sci., 31(3), 674-701, https://doi.org/10.1175/1520-0469(1974)031<0674:IOACCE>2.0.CO;2, 1974.

473 Arakawa, A. and Wu, C.M.: A unified representation of deep moist convection in numerical modeling of the atmosphere.
474 Part I, J. Atmos. Sci., 70(7), 1977-1992, https://doi.org/10.1175/JAS-D-12-0330.1, 2013.

475 Bechtold, P., Köhler, M., Jung, T., Doblas-Reyes, F., Leutbecher, M., Rodwell, M. J., Vitart, F., and Balsamo, G.: Advances
476 in simulating atmospheric variability with the ECMWF model: From synoptic to decadal time-scales, Q. J. Roy. Meteor.
477 Soc., 134, 1337–1351, https://doi.org/10.1002/qj.289, 2008.

478 Chattopadhyay, R., Goswami, B.N., Sahai, A.K., and Fraedrich, K.: Role of stratiform rainfall in modifying the northward
479 propagation of monsoon intraseasonal oscillation, J. Geophys. Res. Atmos., 114(D19),
480 https://doi.org/10.1029/2009JD011869, 2009.

481 Choudhury, A.D. and Krishnan, R.: Dynamical response of the South Asian monsoon trough to latent heating from
482 stratiform and convective precipitation, J. Atmos. Sci., 68(6), 1347-1363, https://doi.org/10.1175/2011JAS3705.1, 2011.

483 Chun, H.Y. and Baik, J.J.: Momentum flux by thermally induced internal gravity waves and its approximation for large-scale
484 models, J. Atmos. Sci., 55(21), 3299-3310, https://doi.org/10.1175/1520-0469(1998)055<3299:MFBTII>2.0.CO;2, 1998.

485 Clough, S.A., Shephard, M.W., Mlawer, E.J., Delamere, J.S., Iacono, M.J., Cady-Pereira, K., Boukabara, S., and Brown,
486 P.D.: Atmospheric radiative transfer modeling: A summary of the AER codes, J. Quant. Spectrosc. Radiat. Transf., 91(2),
487 233-244, https://doi.org/10.1016/j.jqsrt.2004.05.058, 2005.

Crueger, T., Giorgetta, M.A., Brokopf, R., Esch, M., Fiedler, S., Hohenegger, C., Kornblueh, L., Mauritsen, T., Nam, C., Naumann, A.K., and Peters, K.: ICON-A, the atmosphere component of the ICON earth system model: II. Model evaluation, J. Adv. Model. Earth. Syst., 10(7), 1638-1662, https://doi.org/10.1029/2017MS001233, 2018.

Deng, Q., Khouider, B., and Majda, A.J.: The MJO in a coarse-resolution GCM with a stochastic multicloud parameterization, J. Atmos. Sci., 72(1), 55-74. https://doi.org/10.1175/JAS-D-14-0120.1, 2015.

Deshpande, M., Kanase, R., Krishna, R.P.M., Tirkey, S., Mukhopadhyay, P., Prasad, V.S., Johny, C.J., Durai, V.R., Devi, S. and Mohapatra, M.: Global Ensemble Forecast System (GEFS T1534) evaluation for tropical cyclone prediction over the North Indian Ocean, Mausam., 72(1), 119-128, https://doi.org/10.54302/mausam.v72i1.123, 2021.

ECMWF IFS DOCUMENTATION—Cy43r1 Operational Implementation Part IV: Physical Processes; ECMWF: Reading, UK, 2016.

Fu, X. and Wang, B.: The boreal-summer intraseasonal oscillations simulated in a hybrid coupled atmosphere–ocean model, Mon. Weather. Rev., 132(11), 2628-2649, https://doi.org/10.1175/MWR2811.1, 2004.

Gadgil, S. and Gadgil, S.: The Indian monsoon, GDP and agriculture, Econ. polit. Wkly., 4887-4895, https://www.jstor.org/stable/4418949, 2006.

Ganai, M., Tirkey, S., Krishna, R.P.M., and Mukhopadhyay, P.: The impact of modified rate of precipitation conversion parameter in the convective parameterization scheme of operational weather forecast model (GFS T1534) over Indian summer monsoon region, Atmos. Res., 248, 105185, https://doi.org/10.1016/j.atmosres.2020.105185, 2021.

Giorgetta, M.A., Brokopf, R., Crueger, T., Esch, M., Fiedler, S., Helmert, J., Hohenegger, C., Kornblueh, L., Köhler, M., Manzini, E., and Mauritsen, T.: ICON-A, the atmosphere component of the ICON earth system model: I. Model description, J. Adv. Model. Earth. Syst., 10(7), 1613-1637, https://doi.org/10.1029/2017MS001242, 2018.

Han, J. and Pan, H.L.: Revision of convection and vertical diffusion schemes in the NCEP Global Forecast System, Weather. Forecast., 26(4), 520-533, https://doi.org/10.1175/WAF-D-10-05038.1, 2011.

Han, J., Witek, M.L., Teixeira, J., Sun, R., Pan, H.L., Fletcher, J.K., and Bretherton, C.S.: Implementation in the NCEP GFS of a hybrid eddy-diffusivity mass-flux (EDMF) boundary layer parameterization with dissipative heating and modified stable boundary layer mixing, Weather. Forecast., 31(1), 341-352, https://doi.org/10.1175/WAF-D-15-0053.1, 2016.

Han, J., Wang, W., Kwon, Y.C., Hong, S.Y., Tallapragada, V., and Yang, F.: Updates in the NCEP GFS cumulus convection schemes with scale and aerosol awareness, Weather. Forecast., 32(5), 2005-2017, https://doi.org/10.1175/WAF-D-17-0046.1, 2017.

Held, I.M. and Suarez, M.J.: A proposal for the intercomparison of the dynamical cores of atmospheric general circulation models, Bull. Am. Meteorol. Soc., 75(10), 1825-1830, https://doi.org/10.1175/1520-0477(1994)075<1825:APFTIO>2.0.CO;2, 1994.

Hersbach, H. and Dee, D.: ERA5 reanalysis is in production. ECMWF Newsletter No. 147, ECMWF,Reading,UnitedKingdom,7, http://www.ecmwf.int/sites/default/files/elibrary/2016/16299-newsletter-no147-spring-2016.pdf, 2016.

Hoffman, R.N., Kumar, V.K., Boukabara, S.A., Ide, K., Yang, F., and Atlas, R.: Progress in forecast skill at three leading global operational NWP centers during 2015–17 as seen in summary assessment metrics (SAMs), Weather. Forecast., 33(6), 1661-1679, https://doi.org/10.1175/WAF-D-18-0117.1, 2018.

Huffman, G.J., Stocker, E.F., Bolvin, D.T., Nelkin, E.J., and Tan, J.: GPM IMERG Final Precipitation L3 Half Hourly 0.1 degree x 0.1 degree V06, Greenbelt, MD, Goddard Earth Sciences Data and Information Services Center (GES DISC), Accessed: 20 March 2023, doi:10.5067/GPM/IMERG/3B-HH/06, 2019.

Iacono, M.J., Mlawer, E.J., Clough, S.A., and Morcrette, J.J.: Impact of an improved longwave radiation model, RRTM, on the energy budget and thermodynamic properties of the NCAR community climate model, CCM3, J. Geophys. Res. Atmos., 105(D11), 14873-14890, https://doi.org/10.1029/2000JD900091, 2000.

Jiang, X., Li, T., and Wang, B.: Structures and mechanisms of the northward propagating boreal summer intraseasonal oscillation, J. Clim., 17(5), 1022-1039, https://doi.org/10.1175/1520-0442(2004)017<1022:SAMOTN>2.0.CO;2, 2004.

Kanase, R., Tirkey, S., Deshpande, M., Krishna, R.P.M., johny, C.J., Mukhopadhyay, P., Iyengar, G., and Mohapatra, M.: Evaluation of the Global Ensemble Forecast System (GEFS T1534) for the probabilistic prediction of cyclonic disturbances over the North Indian Ocean during 2020 and 2021, J. Earth. Sys. Sci., 132-143, https://doi.org/10.1007/s12040-023-02166-2, 2023.

Kim, Y.J. and Arakawa, A.: Improvement of orographic gravity wave parameterization using a mesoscale gravity wave model, J. Atmos. Sci., 52(11), 1875-1902, https://doi.org/10.1175/1520-0469(1995)052<1875:IOOGWP>2.0.CO;2, 1995.

Kinter, J. L., III, Cash, B., Achuthavarier, D., Adams, J., Altshuler, E., Dirmeyer, P., Doty, B., Huang, B., Jin, E. K., Marx, L., Manganello, J., Stan, C., Wakefield, T., Palmer, T., Hamrud, M., Jung, T., Miller, M., Towers, P., Wedi, N., Satoh, M., Tomita, H., Kodama, C., Nasuno, T., Oouchi, K., Yamada, Y., Taniguchi, H., Andrews, P., Baer, T., Ezell, M., Halloy, C., John, D., Loftis, B., Mohr, R., & Wong, K.: Revolutionizing Climate Modeling with Project Athena: A Multi-Institutional, International Collaboration. Bull. Am. Meteorol. Soc., 94(2), 231-245. https://doi.org/10.1175/BAMS-D-11-00043.1, 2013.

Kumar, S., Arora, A., Chattopadhyay, R., Hazra, A., Rao, S.A., and Goswami, B.N.: Seminal role of stratiform clouds in large-scale aggregation of tropical rain in boreal summer monsoon intraseasonal oscillations, Clim. Dyn., 48, 999-1015, https://doi.org/10.1007/s00382-016-3124-5, 2017.

Kumar, S., Phani, R., Mukhopadhyay, P., and Balaji, C.: Does increasing horizontal resolution improve seasonal prediction of Indian summer monsoon?: A climate forecast system model perspective, Geophys. Res. Lett., 49(7), e2021GL097466, https://doi.org/10.1029/2021GL097466, 2022.

Li, J., Yu, R., Yuan, W., Chen, H., Sun, W. and Zhang, Y.: Precipitation over E ast A sia simulated by NCAR CAM5 at different horizontal resolutions. J. Adv. Model. Earth. Syst., 7(2), 774-790, https://doi.org/10.1002.2014MS000414, 2015.Lott, F. and Miller, M.J.: A new subgrid-scale orographic drag parametrization: Its formulation and testing, Q. J. R. Meteorol. Soc., 123(537), 101-127, https://doi.org/10.1002/qj.49712353704, 1997.

Magnusson, L. and Källén, E.: Factors influencing skill improvements in the ECMWF forecasting system, Mon. Weather. Rev., 141(9), 3142-3153, https://doi.org/10.1175/MWR-D-12-00318.1, 2013.

Majewski, D., Liermann, D., Prohl, P., Ritter, B., Buchhold, M., Hanisch, T., Paul, G., Wergen, W. and Baumgardner, J.: The operational global icosahedral-hexagonal gridpoint model GME: description and high resolution tests, Mon. Wea. Rev., 130, 319– 338, https://doi.org/10.1175/1520-0493(2002)130<0319:TOGIHG>2.0.CO:2, 2002.

Malardel, S., N, Wedi., W, Deconinck., M, Diamantakis., C, Kühnlein., G, Mozdzynski., M, Hamrud. and P, Smolarkiewicz.: A new grid for the IFS, ECMWF Newsletter No. 146, 23–28, 2016.

Mitra, A.K., Prakesh, S., Imranali, M.M., Pai, D.S. and Srivastava, A.K.: Daily merged satellite gauge real-time rainfall dataset for Indian Region, Vayumandal, 40(1-4), 33-43, 2014.

Miura, H., Satoh, M., Nasuno, T., Noda, A. T., and Oouchi, K.: A Madden-Julian Oscillation event realistically simulated by a global cloud-resolving model, Sci., 318(5857), 1763–1765, https://doi.org/10.1126/science.1148443, 2007.

565 Molod, A., Takacs, L., Suarez, M., and Bacmeister, J.: Development of the GEOS-5 atmospheric general circulation model:
566 Evolution from MERRA to MERRA2, Geosci. Model. Dev., 8(5), 1339-1356, https://doi.org/10.5194/gmd-8-1339-205,
567 2015.

568 Mukhopadhyay, P., Prasad, V.S., Krishna, R.P.M., Deshpande, M., Ganai, M., Tirkey, S., Sarkar, S., Goswami, T., Johny,
569 C.J., Roy, K., and Mahakur, M.: Performance of a very high-resolution global forecast system model (GFS T1534) at 12.5
570 km over the Indian region during the 2016–2017 monsoon seasons, J. Earth. Sys. Sci., 128, 1-18,
571 https://doi.org/10.1007/s12040-019-1186-6, 2019.

572 Mukhopadhyay, P., Bechtold, P., Zhu, Y., Murali Krishna, R.P., Kumar, S., Ganai, M., Tirkey, S., Goswami, T., Mahakur,
573 M., Deshpande, M., and Prasad, V.S.: Unraveling the mechanism of extreme (more than 30 sigma) precipitation during
574 August 2018 and 2019 over Kerala, India, Weather. Forecast., 36(4), 1253-1273, https://doi.org/10.1175/WAF-D-20-0162.1,
575 2021.

576 Nastrom, G.D. and Gage, K.S.: A climatology of atmospheric wavenumber spectra of wind and temperature observed by
577 commercial aircraft, J. Atmos. Sci., 42, 950–960, https://doi.org/10.1175/1520-0469(1985)042<0950:ACOAWS>2.0.CO;2,
578 1985.

579 Pan, H.L. and Wu, W.S.: Implementing a mass flux convection parameterization package for the NMC medium-range
580 forecast model. https://repository.library.noaa.gov/view/noaa/11429, 1995.

581 Prakash, S., Mitra, A.K., Momin, I.M., Rajagopal, E.N., Milton, S.F., and Martin, G.M.: Skill of short-to medium-range
582 monsoon rainfall forecasts from two global models over India for hydro-meteorological applications, Meteorol. Appl., 23(4),
583 574-586, https://doi.org/10.1002/met.1579, 2016.

584 Prasad, V.S., Mohandas, S., Gupta, M.D., Rajagopal, E.N., and Dutta, S.K.: Implementation of upgraded global forecasting
585 systems (T382L64 and T574L64) at NCMRWF, In NCMRWF Technical Report, 1-72, 2011.

586 Prasad, V.S., Mohandas, S., Dutta, S.K., Gupta, M.D., Iyengar, G.R., Rajagopal, E.N., and Basu, S.: Improvements in
587 medium range weather forecasting system of India, J. Earth. Sys. Sci., 123, 247-258, https://doi.org/10.1007/s12040-014-
588 0404-5, 2014.

589 Prasad, V.S., Johny, C.J., Mali, P., Singh, S.K., and Rajagopal, E.N.: Global retrospective analysis using NGFS for the
590 period 2000–2011, Current Sci., 370-377, https://www.jstor.org/stable/24912364, 2017.

Rajendran, K., Kitoh, A., Mizuta, R., Sajani, S., and Nakazawa, T.: High-resolution simulation of mean convection and its intraseasonal variability over the tropics in the MRI/JMA 20-km mesh AGCM, J. Clim., 21(15), 3722-3739, https://doi.org/10.1175/2008JCLI1950.1, 2008.

Rao, S.A., Goswami, B.N., Sahai, A.K., Rajagopal, E.N., Mukhopadhyay, P., Rajeevan, M., Nayak, S., Rathore, L.S., Shenoi, S.S.C., Ramesh, K.J., and Nanjundiah, R.S.: Monsoon mission: a targeted activity to improve monsoon prediction across scales, Bull. Am. Meteorol. Soc., 100(12), 2509-2532, https://doi.org/10.1175/BAMS-D-17-0330.1, 2019.

Raymond, D. J.: Convection in the east Pacific Intertropical Convergence Zone, Geophys. Res. Lett., 44, 562-568, doi:10.1002/2016GL071554, 2017.

RSMC Report, Report on Cyclonic disturbances over North Indian Ocean during 2022, India Meteorological Department, https://rsmcnewdelhi.imd.gov.in/report.php?internal_menu=Mjc=

RSMC Report, Report on Cyclonic disturbances over North Indian Ocean during 2023, India Meteorological Department, https://rsmcnewdelhi.imd.gov.in/report.php?internal_menu=Mjc=

Satoh, M., Tomita, H., Miura, H., Iga, S., and Nasuno, T.: Development of a global cloud resolving model-a multi-scale structure of tropical convections, J. Earth. Simul., 3, 11-19, 2005.

Satoh, M., Stevens, B., Judt, F., Khairoutdinov, M., Lin, S.J., Putman, W.M., and Düben, P.: Global cloud-resolving models, Curr. Clim. Change Rep., 5, 172-184, https://doi.org/10.1007/s40641-019-00131-0, 2019.

Skamarock, W.C.: Evaluating Mesoscale NWP Models Using Kinetic Energy Spectra, Mon. Weather. Rev., 132,3019–3032, https://doi.org/10.1175/MWR2830.1, 2004.

Skamarock, W.C., Klemp, J.B., Duda, M.G., Fowler, L.D., Park, S.H., and Ringler, T.D.: A multiscale nonhydrostatic atmospheric model using centroidal Voronoi tesselations and C-Grid staggering, Mon. Weather. Rev., 140(9), 3090–3105, https://doi.org/10.1175/MWR-D-11-00215.1, 2012.

Staniforth, A. and Thuburn, J.: Horizontal grids for global weather and climate prediction models: a review. Q. J. R. Meteorol. Soc., 138(662), 1-26, https://doi.org/10.1002/qj.958, 2012.

Stephens, G.L., L'Ecuyer, T., Forbes, R., Gettelmen, A., Golaz, J.C., Bodas-Salcedo, A., Suzuki, K., Gabriel, P., and Haynes, J.: Dreary state of precipitation in global models, J. Geophys. Res. Atmos., 115(D24), https://doi.10.1029/2010JD014532, 2010.

Sundqvist, H., Berge, E., and Kristjánsson, J.E.: Condensation and cloud parameterization studies with a mesoscale numerical weather prediction model, Mon. Weather. Rev., 117(8), 1641-1657, https://doi.org/10.1175/1520-0493(1989)117<1641:CACPSW>2.0.CO;2, 1989.

Watson, P.A., Berner, J., Corti, S., Davini, P., von Hardenberg, J., Sanchez, C., Weisheimer, A., and Palmer, T.N.: The impact of stochastic physics on tropical rainfall variability in global climate models on daily to weekly time scales, J. Geophys. Res. Atmos., 122(11), 5738-5762, https://doi.org/10.1002/2016JD026386, 2017.

Wedi, N.P., Polichtchouk, I., Dueben, P., Anantharaj, V.G., Bauer, P., Boussetta, S., Browne, P., Deconinck, W., Gaudin, W., Hadade, I., and Hatfield, S.: A baseline for global weather and climate simulations at 1 km resolution, J. Adv. Model. Earth. Syst., 12(11), e2020MS002192, https://doi.org/10.1029/2020MS002192, 2020.

Westra, S., Fowler, H.J., Evans, J.P., Alexander, L.V., Berg, P., Johnson, F., Kendon, E.J., Lenderink, G., and Roberts, N.: Future changes to the intensity and frequency of short-duration extreme rainfall, Rev. Geophys., 52(3), 522-555, https://doi.10.1002/2014RG000464, 2014.

Zhang, G.J.: Convective quasi-equilibrium in the tropical western Pacific: Comparison with midlatitude continental environment, J. Geophys. Res. Atmos., 108(D19), https://doi.org/10.1029/2003JD003520, 2003.

Zhao, Q. and Carr, F.H.: A prognostic cloud scheme for operational NWP models, Mon. Weather. Rev., 125(8), 1931-1953, https://doi.org/10.1175/1520-0493(1997)125<1931:APCSFO>2.0.CO;2, 1997.